NANO · MICRO small
www.small-journal.com

Charged Layered Boron Nitride-Nanoflake Membranes for Efficient Ion Separation and Water Purification

*Aaditya Pendse, Semih Cetindag, Meng-Hsuan Lin, Angelina Rackovic, Rousan Debbarma, Soroush Almassi, Brian P. Chaplin, Vikas Berry, Jerry W. Shan, and Sangil Kim**

2D layered nanomaterials have attracted considerable attention for their potential for highly efficient separations, among other applications. Here, a 2D lamellar membrane synthesized using hexagonal boron nitride nanoflakes (h-BNF) for highly efficient ion separation is reported. The ion-rejection performance and the water permeance of the membrane as a function of the ionic radius, ion valance, and solution pH are investigated. The nonfunctionalized h-BNF membranes show excellent ion rejection for small sized salt ions as well as for anionic dyes (>97%) while maintaining a high water permeability, ≈1.0×10^{-3} L m m^{-2} h^{-1} bar^{-1}). Experiments show that the ion-rejection performance of the membrane can be tuned by changing the solution pH. The results also suggest that the rejection is influenced by the ionic size and the electrostatic repulsion between fixed negative charges on the BN surface and the mobile ions, and is consistent with the Donnan equilibrium model. These simple-to-fabricate h-BNF membranes show a unique combination of excellent ion selectivity and high permeability compared to other 2D membranes.

Since the discovery of graphene in 2004, the family of 2D materials has grown. These materials are known to have interesting physical, chemical, and electronic properties, which can vary significantly from their 3D counterparts. The variation of these properties is attributed to the dimensionality effect and modulation in their band structure. Due to these unique properties, 2D nanostructures have been used in a variety of applications such as high-performance sensors,[1] electronics,[2] catalysis,[3] inert coatings,[4] gas,[5] and ion separation.[6] Of these applications, the performance shown by 2D materials as membrane structures in separation processes stands out because of their high solute rejection and solvent transport properties. Therefore, the synthesis of novel 2D nanostructures is one of the most intensively studied research areas in the development of high-performance separation membranes.

Most 2D materials typically have a layered geometry where the atoms are linked by strong in-plane covalent bonds, while the two adjacent layers are held together by van der Waals forces.[7] Exfoliated nanosheets typically show a high surface-area-to-thickness ratio, which is instrumental in improving the adsorption capacity or the ion selectivity, both of which can lead to a better separation performance. In addition to highly effective ion-rejection properties, 2D membranes are also known to possess excellent water permeability. Due to these properties, many 2D materials such as nm-thick graphitic carbon nitride (g-C_3N_4) nanosheets,[8] MoS_2 sheets,[9] WS_2 nanosheets,[6] graphene,[10] Mxene nanosheets,[11] and graphene oxide (GO),[12] have been recently used as the building blocks for fabricating ultrathin layered membranes for separation applications. These 2D membranes have shown highly efficient size-selective ion separation and high water permeance.

Hexagonal boron nitride (h-BN), so-called "white graphene," is however one of the promising 2D materials that has not been utilized to its full potential in ion-separation applications. For efficient ion separation, the membrane should show high ion selectivity, which is primarily dependent on the channel size and surface charge on the membrane. The h-BN material is known to have a high surface charge density resulting from the adsorption of the hydroxyl ions on the surface defect sites.[13] It also shows excellent oxidation and corrosion resistance, which is an important property for wastewater treatment applications. The high chemical stability of h-BN also enables it to be resistant to chemical cleaning, which is frequently needed during separation processes. Qin et al. reported high ionic conductivities for h-BN nanofluidic channels, prepared by the one-step BN exfoliation method and amine functionalization.[14] More recently, Chen et al. developed a 2D h-BN membrane by functionalizing h-BN flakes (h-BNF) with amino groups to overcome its poor water dispersibility. The functionalized h-BNF membranes demonstrated fast solvent transport and good ion-rejection properties, based on molecular sieving mechanism.[15] However, these membranes do not show charge-based (Donnan) exclusion, due to the amine functionalization of the

A. Pendse, M.-H. Lin, A. Rackovic, R. Debbarma, S. Almassi, Prof. B. P. Chaplin, Prof. V. Berry, Prof. S. Kim
Department of Chemical Engineering
University of Illinois at Chicago
Chicago, IL 60607, USA
E-mail: sikim@uic.edu

S. Cetindag, Prof. J. W. Shan
Department of Mechanical and Aerospace Engineering
Rutgers University
Piscataway, NJ 08854, USA

The ORCID identification number(s) for the author(s) of this article can be found under https://doi.org/10.1002/smll.201904590.

DOI: 10.1002/smll.201904590

surface. There appears to be an opportunity to take advantage of the unique, high-surface-charge properties of boron nitride in aqueous solution to maximize the ion-separation performance of the 2D h-BN membranes via a combination of surface-charge effects and molecular sieving.

The main objective of this study is to investigate the ion-transport properties of a 2D lamellar membrane comprising of a few nm-thick h-BN flakes and evaluate its potential application for water purification. A highly efficient ion-selective 2D membrane was fabricated by depositing exfoliated nm-thick h-BNF without surface functionalization on an anodized alumina oxide (AAO) membrane support. We studied the ion-separation performance of the h-BNF membrane by testing the rejection of various salts and dyes. The effect of solution pH, ion valence and ion radius on the ion separation efficiency of the membrane was also investigated. The 2D h-BNF membrane showed a high ion rejection value, >97%, for the anionic dyes with a slight decrease in the separation performance for the small sized salt molecules. Our results however demonstrate that the ion-exclusion properties of the h-BN agree with a Donnan equilibrium model for the case of the large and the small sized ions, distinct from prior work on amine-functionalized h-BN membranes. This provides a strong indication that the ion rejection in our membrane are governed both by electrostatic interaction and molecular sieving. The 2D h-BNF membranes therefore show the potential to be highly efficient membranes for a variety of water purification applications.

Figure 1a,b shows the atomic force microscopy (AFM) data for the fabricated h-BN nanoflakes. The thickness of the original h-BN flake was around 20 nm (data is not shown here). After the sonication-assisted exfoliation process, it is seen that the thickness of the single exfoliated h-BN nanoflake is about ≈4 nm, which indicates that ≈10–12 atom-thick BN layers were stacked together in a single flake.[16] Several fractured pieces of around a hundred nanometers in size were observed, as well as larger flakes greater than 300–400 nm in lateral dimensions. This indicates that the exfoliation process reduces the thickness of the original BN particle from ≈20 to ≈4 nm, while maintaining a large lateral size. The high aspect ratio of the flakes significantly increases the surface area of the flow channels, which can improve the membrane separation performance. The scanning electron microscopy (SEM) data in Figure 1c,d shows that the individual BN nanosheets are parallelly interlocked with each other to form a tightly packed lamellar structure. The cross-sectional SEM image shows that a BNF membrane with a thickness of around 10 µm has been fabricated (Figure 1d). In order to measure the nanofludic channel width between the BNFs, we conducted size exclusion tests using slightly charged 5 nm gold (Au) nanoparticles coated with polyvinylpyrrolidone (PVP). UV–vis spectra analysis of the permeate solution shows that the BNF membrane completely rejected the 5 nm Au particles (Figure S1 in the Supporting Information). The results from the Au-nanoparticle permeation test prove that nm-wide (<5 nm) flow channels are present between the overlapping flakes and serve as the nanofluidic channels for ion separation. Figure 1e schematically illustrates that this compact structure and the sub 5 nm flow channels of the BNF membrane can enable high water flux and the enhanced the ion-separation properties of the membrane.

The X-ray diffraction (XRD) patterns recorded for the wet and the dry h-BN powder show an expected peak at 26.76° resulting from the (002) plane in the h-BN structure (Figure S2 in the Supporting Information). Peaks corresponding to any of the other phases of h-BN were not observed, showing that the crystal structure of the powder remains unchanged during the exfoliation and deposition process. The data obtained from the XRD measurements are used to theoretically calculate the lattice spacing between the BN particles using Bragg's law

$$N\lambda = 2d\sin\theta \tag{1}$$

where λ (0.154 nm) is the wavelength of the incident light, d is the lattice spacing, and θ is the diffraction angle. The space between the lattice can exert a strong capillary force, pulling the fluid inside. This would result in the formation of additional flow channels, which would affect the rejection through the membrane. However, the lattice spacing values (≈0.33 nm) and the peak position (≈27°) of the wet and dry samples are almost identical (Table S1 in the Supporting Information). This result indicates that there is negligible water uptake taking place in the interspace of the lattice structure.[14] Therefore, it is assumed that the interlayer spaces created due to the overlapping of the h-BN nanoflakes are the major channels responsible for the ionic-screening effect.

To evaluate ionic separation performance of the h-BN membranes, we used various ions with different hydrated radius and valance: pyrenetetrasulfonic acid tetrasodium salt (Na_4PTS; $z^-/z^+ = 4$, $r_{PTS^{4-}} = 5.04$ Å[17]), potassium ferricyanide (PFCN; $z^-/z^+ = 3$, $r_{FCN^{3-}} = 4.75$ Å[17]), naphthalene-di-sulfonic acid disodium salt (NDS; $z^-/z^+ = 2$, $r_{NDS^{2-}} = 4.25$ Å[18]), potassium sulfate (K_2SO_4; $z^-/z^+ = 2$, $r_{SO_4^{2-}} = 3.79$ Å[17]), magnesium sulfate ($MgSO_4$; $z^-/z^+ = 1$, $r_{SO_4^{2-}} = 3.79$ Å[17]), sodium chloride (NaCl; $z^-/z^+ = 1$, $r_{Cl^-} = 3.32$ Å[17]) and ruthenium-tris(2,2′-bipyridyl) dichloride (Rubipy; $z^-/z^+ = 0.5$, $r_{Rubipy^{2+}} = 5.90$ Å[17]). **Figure 2**a and Table S2 in the Supporting Information indicate that ion rejection increases as its hydrated radius increases demonstrating molecular sieving properties of the h-BN membranes (Na_4PTS > PFCN > NDS > K_2SO_4 > NaCl). Rejection for NaCl is lower than 40%, however, ion rejection performance of the membrane starts increasing for ions with hydrated radii close to 4 Å[17,18] (R = 78% for SO_4^{2-} and R = 80% for NDS^{2-}). The rejection for ions larger than 4.5 Å[17] further increases and the membrane demonstrates its high ion rejection performance for FCN^{3-} (R = 95%) and PTS^{4-} (R = 98%). However, the h-BN membrane exhibits a low ion rejection of ≈20% for Rubipy ($z^-/z^+ = 0.5$), although its hydrated radius is larger than PTS^{4-}.[17] This results suggest that electrostatic interaction of ions with the negatively charged membrane surface also plays important role in ion rejection properties of the h-BN membrane.

In order to explain the effect of surface charge on ion rejection performance, we first investigated the pH-dependent separation performance of the h-BNF membrane because the solution pH is known to have a prominent impact on the surface charge of single-layered BN sheets, which would alter the selectivity of the lamellar membrane.[12a,19] The rejection of 0.5×10^{-3} M PFCN versus the pH is shown in Figure 2b. At relatively low pH (pH = 3), the membrane shows an ion rejection of ≈10%. The rejection increases sharply as the pH is increased beyond 3, and stabilizes for a pH > 9, with a maximum ion rejection

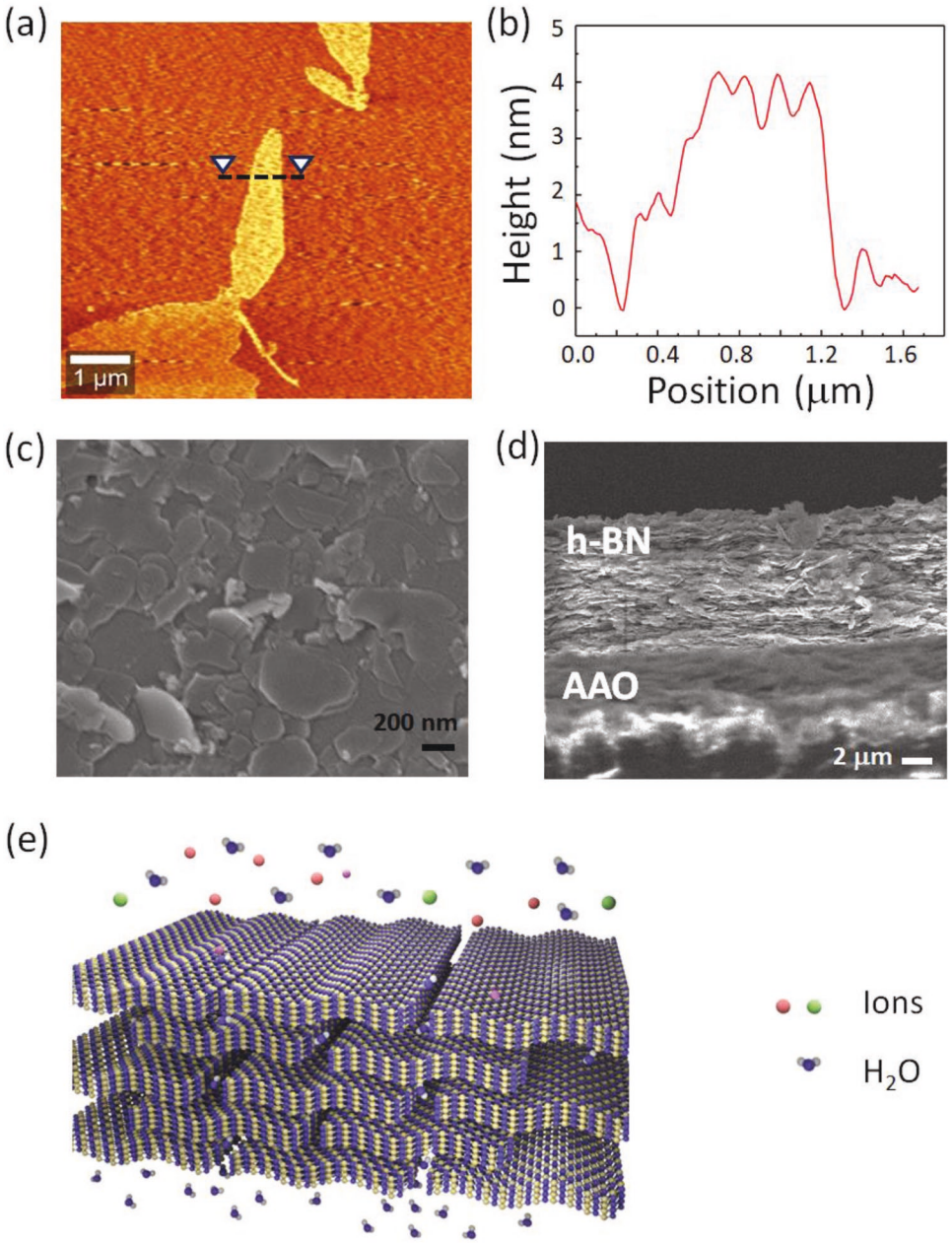

Figure 1. a) AFM topographic image of a representative h-BN flake (h-BNF), b) AFM height profile plot corresponding to the dotted line, FE-SEM images of the c) top view and the d) cross section view of the layered BN membrane. e) Schematic showing that the BNF membrane transports water molecules while rejecting ions.

of ≈97.5% for the PFCN solution. To explain these results, we experimentally measured zeta potentials, ζ, for the h-BNF as a function of pH (Figure S3 in the Supporting Information). The h-BNF powder shows its maximum value ($\zeta = -60$ to -70 mV) at pH = 8–10, which is close to values reported from boron nitride nanotubes[13] and other h-BN powders.[14,20] The negative surface charge of the h-BNF is believed to be due to the adsorption of hydroxyl ions on the surface of the h-BN.[13] Results from an ab initio simulation demonstrate that an activated boron site that is, one with a hydrogen atom bound to a nitrogen atom, can seed water dissociation on a h-BN surface ($BN_3 + H_2O \leftrightarrow BN_3\text{-}OH^- + H^+$).[13] At a higher pH, more hydroxyl ions are present in the solution leading to an increased adsorption on the h-BN surface, which consequently increases the surface charge density. Thus, a stronger electrostatic repulsion exists between the membrane fixed charges and the mobile ions, resulting in a higher potential for ion-rejection at high pH. This improvement in the separation performance continues until the membrane reaches a saturation point around pH = 9. Beyond this point, there are likely no more adsorption sites available for the hydroxyl bonding, which stabilizes the surface charge on the BN sheets. Therefore, the membrane reaches its maximum rejection capacity, which is reflected by the plateau in the measured ion-rejection curve after pH = 9. Unlike the

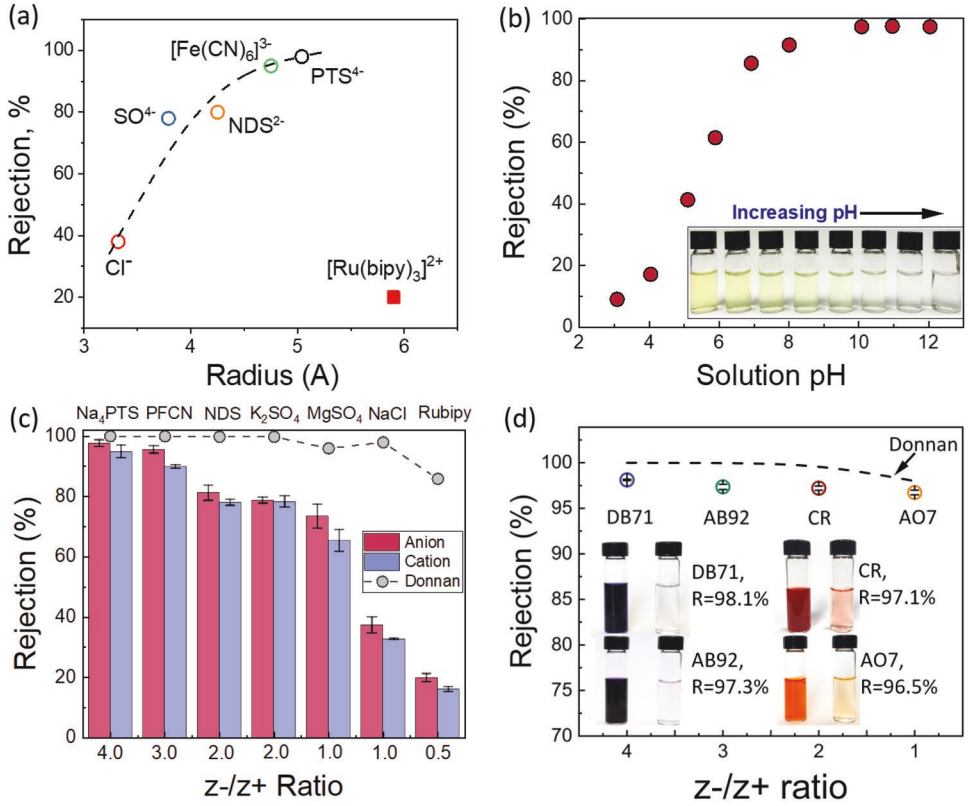

Figure 2. a) Effect of the hydrated radius on the salt rejection through the h-BNF membrane, b) effect of solution pH on the rejection of the potassium ferricyanide solution by the h-BN membrane, Effect of z^-/z^+ ratio of the c) salts and d) dyes on the rejection properties of the h-BN membrane ($C_{feed} = 0.5 \times 10^{-3}$ M, pH 10).

rejection, the permeance through the membrane is seen to be independent of solution pH. An average permeability of ≈1.0×10^{-3} L m m^{-2} h^{-1} bar^{-1} (120 L m^{-2} h^{-1} bar^{-1} of permeance for 10 µm layer thickness) is observed for all the experiments.

Considering the role of the electrostatic interactions, the valence of the anionic and the cationic species in the solution is also known to have a significant effect on the rejection through the charged membrane.[21] Indeed, as shown in Figure 2c, the ion exchange chromatography analysis shows a decrease in the anion and the cation rejection with the z^-/z^+ ratio. The lower rejection of Rubipy despite the large hydrated radius can therefore be explained by the Donnan charge exclusion theory. The Donnan theory describes the rejection coefficients of the ions permeating through the charged membrane according to the following equation

$$R = 1 - \frac{c_i^m}{c_i} = 1 - \left(\frac{|z_i| c_i}{|z_i| c_i^m + c_x^m} \right)^{|z_i/z_i|} \quad (2)$$

where c_i and c_i^m are the concentrations of co-ions in the solution and in the membrane phase, respectively, c_x^m is the membrane charge concentration, z is the ion valence, and subscripts i and j indicate co-ions and counterions, respectively. Equation (2) predicts that the rejection through the membrane will decrease exponentially with a decrease in the z^-/z^+ ratio, because the salt rejection through the membrane is influenced by the balance between the electrostatic forces of the anions and the cations in the solution. The negative charges on the membrane surface repel the anions while attracting the cations, which leads to a separation of the ions in the bulk and membrane phase. The electroneutrality condition, however, restricts the independent migration of the ionic species and requires them to transport as ion pairs. The anion with the higher valence experiences a greater repulsive force from the charged surface, which makes it difficult for it to pass through the membrane, resulting in a higher overall salt rejection. As the valence of the anion decreases, the cations can screen the surface charges more effectively, thus facilitating anion permeation,[21] which leads to a decrease in the overall salt rejection. Figure 2c shows the comparison between the experimental results of the salt rejection performance and the theoretical values predicted by the Donnan model. Considering the molecular sieving based separation mechanism, Rubipy is expected to show a significantly high rejection value owing to the hydrated radius of 0.590 nm. However, as explained by the Donnan charge exclusion theory, the divalent cation in the Rubipy molecule effectively screens the negative surface charges thus allowing an increased salt flow through the membrane, which decreases the overall rejection performance. Our results agree with the separation performance of the negatively charged carbon nanotube membranes,[21] where significantly low rejection values are seen for the salts with the $z^-/z^+ < 1$. In addition, the Donnan model predicts a lower $MgSO_4$ rejection as compared to NaCl because

the divalent Mg^{2+} is expected to screen the negative surface charges more effectively as compared to the monovalent Na^+, thus allowing the SO_4^{2-} ions to flow through the membrane. However, the model does not consider the effect of the ion size on the rejection properties. We believe that the larger size of the SO_4^{2-} ion as compared to the Cl^- ion is primarily responsible for the higher $MgSO_4$ rejection which can be observed in many other NF membranes.[22] The increase in the rejection performance with the hydrated radius, as well as the pH-dependent rejection data suggest that both, the molecular sieving as well as the electrostatic repulsion govern the transport of the ionic species through the h-BNF membrane. To confirm this speculation, we further measured the separation performance of larger-sized anionic dye molecules with varying z^-/z^+ ratios through the h-BNF membrane: Direct Blue 71 (DB71; 3.0 nm × 1.5 nm × 1 nm), acid blue 92 (AB92; 1.43 nm × 1.36 nm × 0.9 nm), congo red (CR; 2.5 nm × 0.7 nm), and acid orange 7 (AO7; 0.73 nm × 1.36 nm × 0.23 nm). As shown in Figure 2d, clear or weakly colored permeate solutions were obtained after the filtration of the 0.5×10^{-3} M dye solution (DB71, AB92, CR, and AO7), suggesting a very high rejection of the analytes. In addition, UV–vis spectroscopy analysis (Figure S4 in the Supporting Information) showed 95–98% ion rejection for all tested anionic dye solutions. The results with dye solutions show a significantly higher rejection performance as compared to the salts with the same z^-/z^+ ratio, which can be attributed to the larger size of the dye molecules and, as predicted the Donnan model, an increase in the dye rejection is seen with the increase in the z^-/z^+ ratio (Figure 2d). Our results thus provide strong evidence for the claim that ion rejection in the 2D h-BNF membrane is a result of the combined effect of the ionic size and the electrostatic interactions between the ions and the charged membrane surface. Similar to the varying solution basicity, the change in the ion valence ratio and the ion size shows a negligible impact on the membrane permeance (Figure S5 in the Supporting Information). Minor fluctuations are seen in the permeance values which are well within the acceptable error ranges. From the results of the 5 nm Au nanoparticle and Rubpy ion (1.18 nm of hydrated diameter) filtration tests, we can estimate ≈1.2–5.0 nm width for the flow channel between BNFs.

In order to fabricate an efficient separation membrane, it is highly desirable to have an optimized thickness to balance flux and rejection. Thick membrane has low water flux despite high rejection rate, while a thinner membrane usually shows higher flux but lower rejection and may suffer from mechanical problems. The thickness-dependent separation performance of BNF membranes is shown in **Figure 3**a. The thickness of the membranes was controlled by the volume of the BN flake dispersion deposited on the AAO support and was measured using optical microscope. PFCN molecules were used as a probe to investigate the rejection performance of the BNF membranes with different thicknesses. The water permeance decreases about twofold as the thickness increase from 2 to 10 μm. The 7.2 μm thick BNF membrane shows a 92.7% rejection of the PFCN molecules and water permeance of ≈135 L m^{-2} h^{-1} bar^{-1}. In addition, we also measured the dependence of the separation performance of BNF membranes on the applied pressure. Figure 3b shows a slight increase in the rejection with a slight loss in the membrane permeance with increase in the applied pressure. Meanwhile, the increase in the applied pressure from 40 to 60 psi induces ≈1.5% increase in the rejection. This result suggests that the increased pressure slightly affects compaction of the BN flakes thus nanofluidic pathway is dimensionally stable. Further, to investigate performance stability of the h-BNF membrane, the permeance and the rejection of the PFCN solution at pH 10 was measured over a period of 2 days. As shown in Figure 3c, water permeance of ≈135 L m^{-1} h^{-1} bar^{-1} and the rejection ≈92% for the h-BNF membrane are stable throughout the 48 h of operation. This stable water permeation and separation performance suggest that almost no clogging occurs in the membrane.

Finally, the ion separation performance of the 2D h-BNF membranes is compared with the other 2D membranes including functionalized h-BN,[15] graphene derivatives,[12,23] exfoliated dichalcogenides,[6,9] and Mxene[11] (Figure 3d,e and Table S3 in the Supporting Information). Comparing to other 2D membranes, our h-BNF membrane shows an excellent small anion (e.g., PFCN, K_2SO_4, and $MgSO_4$) separation performance resulting from the combination of tightly packed membranes structure and high surface charge of the h-BNF, which has not been previously exploited in (amine-functionalized) h-BNF membranes. Thickness of the h-BNF membrane is ≈7 μm, which can be potentially optimized to typical thickness of NF membranes (<1 μm). Thus, it is also reasonable to express water flux of membrane with thickness-normalized permeance (permeability), which can offer good information on intrinsic water transport properties of membrane materials. Figure 3e shows the separation performance of the 2D membranes in terms of membrane permeability, our h-BNF membranes demonstrate a unique combination of both high ion rejection and permeability, $>1.0 \times 10^{-3}$ L m m^{-2} h^{-1} bar^{-1}, for PFCN, thus outperforming all other 2D membranes.

In summary, 2D h-BN nanosheets having high surface charge were utilized for the fabrication of lamellar membranes for the ion-selective separation of salt and the dye molecules. The performance of the h-BNF membrane was investigated as a function of the solution pH, ion size, and anion to cation valence ratio. Our membrane shows a significantly high rejection performance for all the anionic dyes and the salts while maintaining a stable water permeance. The membrane-rejection performance of the salt solutions is seen to increase with the hydrated radius of the salt ions, which indicates a molecular sieving based separation mechanism. The pH-dependent rejection shows a similar trend to the zeta-potential curve suggesting that the electrostatic interactions also contribute to the rejection through the h-BNF membranes. This result is further confirmed by the low rejection of the cationic Rubipy ions despite the large hydrated radius. We can therefore conclude that the significantly high separation performance of the h-BNF membranes results from a combination of the molecular sieving as well as the electrostatic repulsion effect owing to the tightly packed flake structure and the high surface charge density of h-BNF. These h-BNF membranes, having excellent rejection and permeability performance as well as a simple and scalable fabrication process, therefore show great potential for various separation applications.

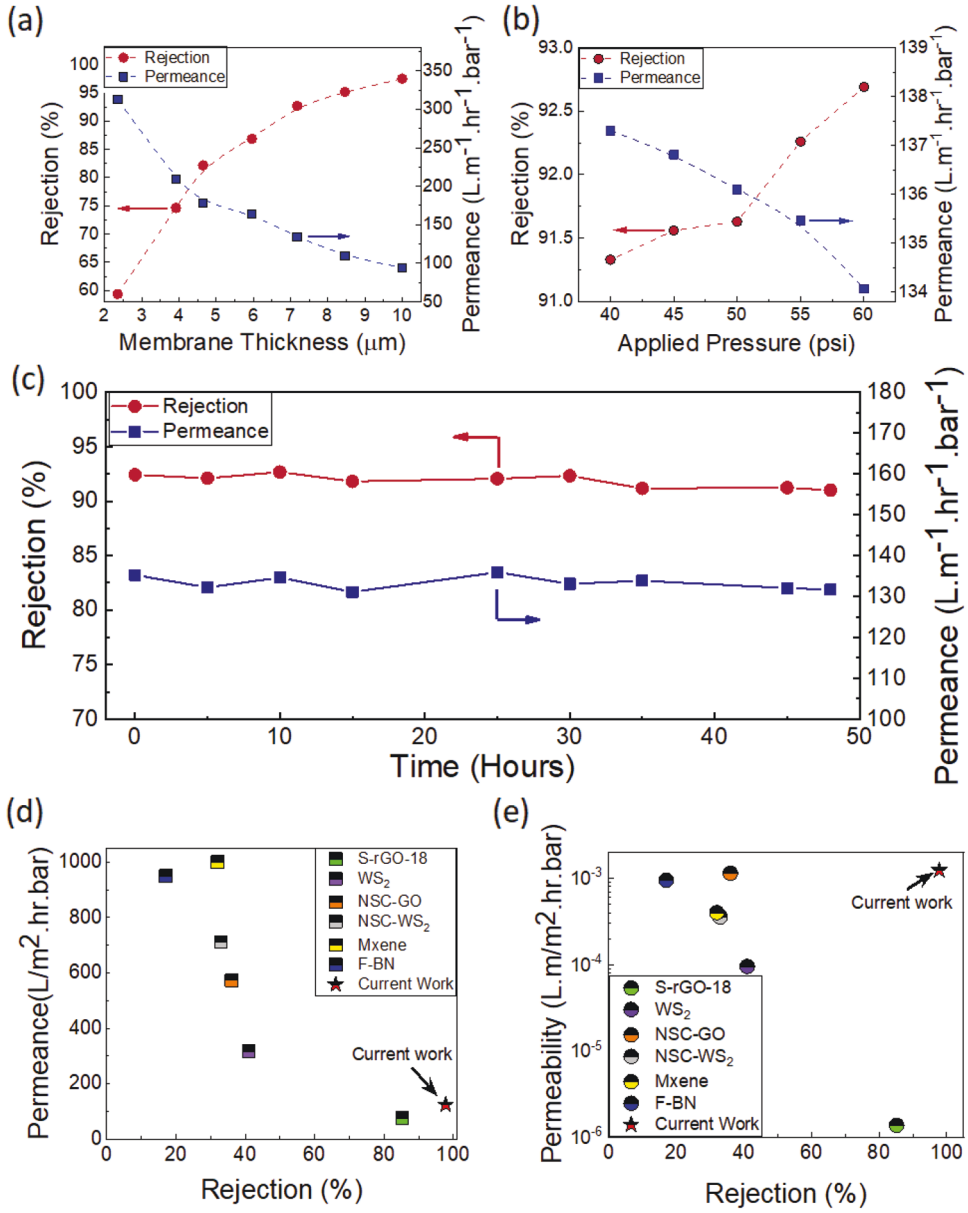

Figure 3. The effect of a) membrane thickness and b) applied pressure on the filtration through the BNF membrane, c) permeance and rejection performance of the potassium ferricyanide solution ($C_{feed} = 0.5 \times 10^{-3}$ M, pH 10) through BNF membrane measured over 2 days, Comparison of ion (PFCN) separation performance of the 2D h-BN membrane with respect to d) permeance and e) permeability with other 2D membranes: S-rGO-18,[12b] WS_2,[6] NSC-GO,[12a] NSC-WS_2,[6] Mxene,[11] and F-BN.[15]

Experimental Section

Materials: Boron nitride powder (99.8% purity, 300 nm thickness, and 3–8 μm lateral dimension) was obtained from US Research Nanomaterials, Inc., and AAO membranes (100 nm pore size) were purchased from Sterlitech Corporation. 5 nm Au nanoparticles functionalized with polyvinylpyrrolidone (5 mV of zeta potential) was purchased from Nanocomposix. Pyrenetetrasulfonic acid tetrasodium salt (Na_4PTS), 2, 6-naphthalene-di-sulfonic acid disodium salt (NDS), potassium sulfate (K_2SO_4), magnesium sulfate ($MgSO_4$), sodium chloride (NaCl), potassium ferricyanide (≥99%), direct blue 71 (≥50%), congo red (≥78.8%), acid orange 7 (≥90%), ruthenium-tris(2,2′-bipyridyl) dichloride (99.9%), potassium hydroxide (≥85% purity), and hydrochloric acid (37% wt/wt) were purchased from Sigma Aldrich. Acid Blue 92 dye (≥99%) was purchased from Tokyo Chemical Industry Co., Ltd. (TCI–America). All the solutions were prepared in Barnstead NANOpure deionized water (DI) (18.2 MΩ cm).

Membrane Fabrication: Simple sonication-assisted liquid exfoliation of bulk h-BN powder was employed to prepare nm-thick BNF layers.[24] These exfoliated BNF layers were then deposited on an AAO membrane support for the fabrication of the 2D h-BNF membrane. The h-BNF solution was prepared by mixing h-BN powder with isopropyl alcohol (1.8 mg mL^{-1} loading) and then sonicated with a tip sonicator (Misonix 3000) for 80 min, followed by bath sonication (Fisher Scientific FS60) for 24 h at 20 °C. The h-BN flakes had zeta potentials more than 30 mV (Figure S3 in the Supporting Information) for all pH > 4, showing the good stability of the dispersion. The resulting milky-white h-BNF suspension was centrifuged at 3500 rotations per minute (rpm) for 30 min and the supernatant (top 70–80% of the solution) was collected and filtered using a polyvinylidene fluoride (PVDF) membrane (0.45 μm

pore size) to obtain properly exfoliated h-BN sheets for the fabrication of the layered membrane. A vacuum filtration apparatus aided in the deposition of the BN nanoflakes on the AAO membrane support. The AAO membrane support was mounted across a filtration setup and the fine h-BN nanoflakes were deposited on the AAO membrane by applying a vacuum pressure of ≈1 bar across the membrane and then air dried for 2 h and stored in wet state in DI water prior to characterization.

Membrane Characterization: Field emission scanning electron microscopy (FIB–FEI Quanta 400F system, Thermo Scientific) was used to image the top surface as well as the layered structure of a cross-section of the prepared membranes. The nanometer scale thickness of the individual h-BN nanoflake was determined using atomic force microscopy. The sample was prepared by the drop-casting technique using diluted colloidal suspension on a clean silicon surface. A combined confocal Raman-atomic force microscope (Raman-AFM, WITEC α-300RA) was used for the characterization of the h-BN nanoflakes. Tapping mode AFM images were obtained using a silicon probe with an aluminum reflex coating.

The crystal structure of the h-BN nanoflakes was determined by X-ray diffraction. The filtered h-BN nanoflakes were divided into two samples: i) wet state (the sample as obtained) and ii) dry state (the sample subjected to a vacuum treatment for 24 h to remove all the water content). The measurements were obtained using a Siemens D-5000 X-ray diffractometer, equipped with a α-Cu X-ray tube (40 kV and 25 mA). The scans (0.02° step size and 1 s dwell time) were collected using DataScan software (MDI, v. 4.3.355, 2005).

Zeta potentials were measured using a Brookhaven ZetaPALS instrument after dispersion of the h-BN in solution by sonication. About 1.75 mL of the h-BN suspension was carefully placed into a capillary cell, ensuring that bubbles were not created. The measurement was run at room temperature ($T = 25$ °C) with an applied AC voltage (V) of 5 V and frequency of 10 Hz. Every experiment was repeated five times to calculate the mean value of the experimental data. In all of the measurements, 10×10^{-3} M KCl was used as the background electrolyte and the pH was adjusted using KOH or HCl. In addition to determining the surface charge,[25] the zeta potential measurements are also used to assess the stability of the h-BN suspension. Suspensions showing particles with zeta potentials more positive than +30 mV, or more negative than −30 mV, are normally considered to be stable.[26] The data indicates that stable suspensions are formed for all the solutions above pH = 4. At this pH, the negative charge on the suspended particles becomes large enough to repel the neighboring particle, which prevents coagulation.

Membrane Separation Performance: The ion-transport properties of the prepared 2D h-BN membrane were investigated using an Amicon 8050 stirred cell system. Typically, 50 mL of 0.5×10^{-3} M ionic solutions were used for the experiments. The feed solution was stirred constantly at 50 rpm to minimize concentration polarization near the membrane surface. The ion concentration at the feed and the permeate sides was measured using a Ion exchange chromatography for the salt solutions and UV–vis spectrophotometer (UV-1800, Shimadzu) for the dye solutions. Low-concentration electrolyte solutions (0.5×10^{-3} M) were used throughout this study to ensure that the Debye length (λ_D) was large enough (≈19.48 nm) so that a complete double-layer overlap could be achieved within the nanochannels. The permeance, L_P (L m^{2-} h^{-1} bar^{-1}), through the membrane was calculated by the permeate flux, J_p (L h^{-1}), the applied pressure, ΔP (bar), and the membrane area, A (m^2)

$$L_P = \frac{J_P}{A \times \Delta P} \tag{3}$$

Ion rejection, R, was measured by the difference between the concentration of the feed (C_{feed} (mM)) and the permeate ($C_{permeate}$ (mM)) and was defined as follows

$$R(\%) = \left(1 - \frac{C_{permeate}}{C_{feed}}\right) \times 100 \tag{4}$$

The pH sensitivity of ion rejection was analyzed using aqueous potassium ferricyanide solutions (0.5×10^{-3} M) with pH ranging from ≈3 to 13. Hydrochloric acid (1 M) and potassium hydroxide (1 M) solutions were used to adjust the solution pH. The prepared solutions were tested using a stirred cell apparatus, following the procedure described above. The effect of the membrane thickness was analyzed by preparing membranes with different amount of BNF dispersions deposited onto the AAO support. Similarly, the applied feed pressure was maintained at ≈60 psi for all the experiments. All the membranes were refreshed by treating it with a 0.2 wt% solution of HCl for 2 h to remove any traces of ions adsorbed on the h-BN nanoflake surface[27] and stored in a wet state (DI water) until the next experiments.

Supporting Information

Supporting Information is available from the Wiley Online Library or from the author.

Acknowledgements

This work has been supported by a grant from the National Science Foundation (Grant No. CMMI-1762905).

Conflict of Interest

The authors declare no conflict of interest.

Keywords

2D nanosheets, boron nitride, ion selectivity, layered materials, nanostructured membranes

Received: August 15, 2019
Published online: October 10, 2019

[1] K. Lee, R. Gatensby, N. McEvoy, T. Hallam, G. S. Duesberg, *Adv. Mater.* **2013**, *25*, 6699.
[2] J. A. Wilson, F. Di Salvo, S. Mahajan, *Adv. Phys.* **1975**, *24*, 117.
[3] D. Deng, K. Novoselov, Q. Fu, N. Zheng, Z. Tian, X. Bao, *Nat. Nanotechnol.* **2016**, *11*, 218.
[4] R. Mas-Balleste, C. Gomez-Navarro, J. Gomez-Herrero, F. Zamora, *Nanoscale* **2011**, *3*, 20.
[5] a) H. W. Kim, H. W. Yoon, S.-M. Yoon, B. M. Yoo, B. K. Ahn, Y. H. Cho, H. J. Shin, H. Yang, U. Paik, S. Kwon, *Science* **2013**, *342*, 91; b) H. W. Kim, H. W. Yoon, S.-M. Yoon, B. M. Yoo, B. K. Ahn, Y. H. Cho, H. J. Shin, H. Yang, U. Paik, S. Kwon, J.-Y. Choi, H. B. Park, *Science* **2013**, *342*, 91.
[6] L. Sun, Y. Ying, H. Huang, Z. Song, Y. Mao, Z. Xu, X. Peng, *ACS Nano* **2014**, *8*, 6304.
[7] K. Peng, L. Fu, J. Ouyang, H. Yang, *Adv. Funct. Mater.* **2016**, *26*, 2666.
[8] Y. Wang, L. Liu, J. Xue, J. Hou, L. Ding, H. Wang, *AIChE J.* **2018**, *64*, 2181.
[9] L. Sun, H. Huang, X. Peng, *Chem. Commun.* **2013**, *49*, 10718.
[10] F. Zhou, M. Fathizadeh, M. Yu, *Annu. Rev. Chem. Biomol. Eng.* **2018**, *9*, 17.
[11] L. Ding, Y. Wei, Y. Wang, H. Chen, J. Caro, H. Wang, *Angew. Chem., Int. Ed.* **2017**, *56*, 1825.
[12] a) H. Huang, Z. Song, N. Wei, L. Shi, Y. Mao, Y. Ying, L. Sun, Z. Xu, X. Peng, *Nat. Commun.* **2013**, *4*, 2979; b) L. Huang, J. Chen, T. Gao, M. Zhang, Y. Li, L. Dai, L. Qu, G. Shi, *Adv. Mater.* **2016**, *28*, 8669.

[13] A. Siria, P. Poncharal, A.-L. Biance, R. Fulcrand, X. Blase, S. T. Purcell, L. Bocquet, *Nature* **2013**, *494*, 455.
[14] S. Qin, D. Liu, G. Wang, D. Portehault, C. J. Garvey, Y. Gogotsi, W. Lei, Y. Chen, *J. Am. Chem. Soc.* **2017**, *139*, 6314.
[15] C. Chen, J. Wang, D. Liu, C. Yang, Y. Liu, R. S. Ruoff, W. Lei, *Nat. Commun.* **2018**, *9*, 1902.
[16] L. Song, L. Ci, H. Lu, P. B. Sorokin, C. Jin, J. Ni, A. G. Kvashnin, D. G. Kvashnin, J. Lou, B. I. Yakobson, *Nano Lett.* **2010**, *10*, 3209.
[17] R. K. Joshi, P. Carbone, F. C. Wang, V. G. Kravets, Y. Su, I. V. Grigorieva, H. A. Wu, A. K. Geim, R. R. Nair, *Science* **2014**, *343*, 752.
[18] M. Majumder, N. Chopra, B. J. Hinds, *ACS Nano* **2011**, *5*, 3867.
[19] H. Huang, Y. Mao, Y. Ying, Y. Liu, L. Sun, X. Peng, *Chem. Commun.* **2013**, *49*, 5963.
[20] T. Lu, L. Wang, Y. Jiang, C. Huang, *J. Mater. Chem. B* **2016**, *4*, 6103.
[21] F. Fornasiero, H. G. Park, J. K. Holt, M. Stadermann, C. P. Grigoropoulos, A. Noy, O. Bakajin, *Proc. Natl. Acad. Sci. USA* **2008**, *105*, 17250.
[22] a) F. T. Minhas, M. Bhanger, *Procedia Manuf.* **2018**, *17*, 680; b) Y. Zhang, S. Zhang, T.-S. Chung, *Environ. Sci. Technol.* **2015**, *49*, 10235; c) A. Y. Lehi, A. Akbari, H. Soleimani, *Membr. Water Treat.* **2015**, *6*, 173.
[23] Y. Han, Z. Xu, C. Gao, *Adv. Funct. Mater.* **2013**, *23*, 3693.
[24] Y. Lin, T. V. Williams, T.-B. Xu, W. Cao, H. E. Elsayed-Ali, J. W. Connell, *J. Phys. Chem. C* **2011**, *115*, 2679.
[25] M. Elimelech, W. H. Chen, J. J. Waypa, *Desalination* **1994**, *95*, 269.
[26] I. M. Joni, R. Balgis, T. Ogi, T. Iwaki, K. Okuyama, *Colloids Surf. A* **2011**, *388*, 49.
[27] S. Madaeni, S. Samieirad, *Desalination* **2010**, *257*, 80.